The Institute of Space and Astronautical Science
Report No. 616, December 1984

Development of Faraday Cup onboard MS-T5 for Solar Wind Measurement

By

Kohichiro OYAMA, Kazunori AKAI, Kazuyuki NAKAZAWA*,
Kunio HIRAO and Shinriki TEI**

(October 30, 1984)

Summary: Faraday cup which will be installed in Japan's first interplanetary satellite, MS-T5 is now ready to go after three years' developing period. The cup which consists of four grids and ion collector was designed to measure ion density, bulk velocity and ion temperature by utilizing spacecraft spinning. The range of these parameters to be measured are few~several ten ions/cc for ion density, $\sim 10^4$ K for ion temperature and 300 Km~700 km/sec for bulk velocity. Among three parameters to be measured, bulk velocity and ion density can be measured within 10% accuracy. Ion temperature can be obtained within the accuracy of ~20%. What we have done so far are:

(1) To study the basic physics on the ion response to the rapidly changing potential,
(2) To get a theoretical description of ion current versus satellite spin angle,
(3) To check the theoretical equation by means of laboratory experiment and finally
(4) To make the software to process data after the satellite MS-T5 is launched.

The report describes several useful findings which were made clear during the study listed above.

1. PRINCIPLE OF THE MEASUREMENT

Faraday cup can measure bulk velocity (V_b), ion density (N_0) and ion temperature (T_i) by utilizing spacecraft spinning as shown in Fig. 1. When the modulating grid voltage V_{G2} becomes equal to the potential, $m_i/2e(V_b \cos\theta)^2$, the energy corresponding to the component of the incoming ion bulk velocity, which is normal to the electrode plane, ion flux start to be modulated, where θ is the angle which is normal to the electrode with respect to solar wind stream, which is very close to sun-satellite direction. For example, as shown in Fig. 2 when ions which have the bulk velocity of 400 km/sec (which corresponds to the proton energy of ~820 eV) with $T_i=0$ and fly toward the 2nd grid to which $V_{G2}=490$ V is applied, the incoming ions are not retarded by the potential V_{G2} as long as the electrode surface faces the solar wind stream. When the angle becomes 40 degrees as the Faraday cup rotates and the velocity component of the ions which is normal to the electrode plane becomes equal to V_{G2}, the ions start to be blocked. Beyond these angles, the ions continue to be blocked. Therefore the bulk velocity V_b can be obtained if the angle at which modulated ion current starts to appear at the collector is

* Japan Radio Co., Ltd.
** Musashi Institute of Technology.

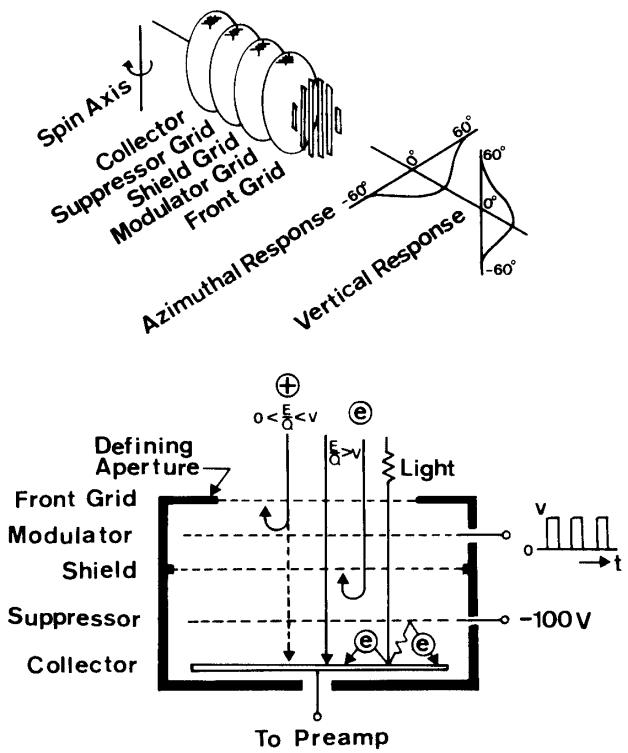

Fig. 1. Principle of the measurement and structure of Faraday cup. It is noted that shielding grid G_3 is very important to block the leakage of high voltage which is applied to the second grid G_2.

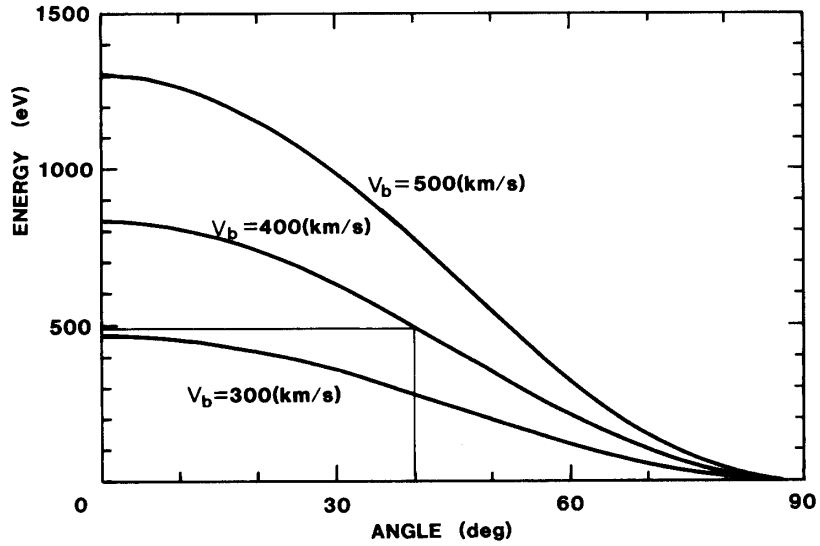

Fig. 2. Changing of the velocity component normal to the electrode plane as spacecraft rotates.

known and V_{G2} is monitored. The ion density is obtained from the collector current intensity. When the T_i has finite value, T_i, N_0 and V_b are obtained by fitting the measured curve to the one which is theoretically described as;

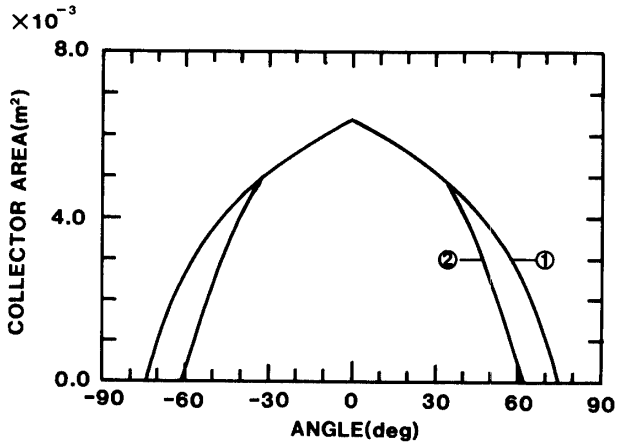

Fig. 3. Collecting surface area S_0 (θ) of flight model Faraday cup.

(1) No obstacle exists in front of the 1st grid.
(2) When Faraday cup is installed in the satellite. Satellite wall decreases the surface area.

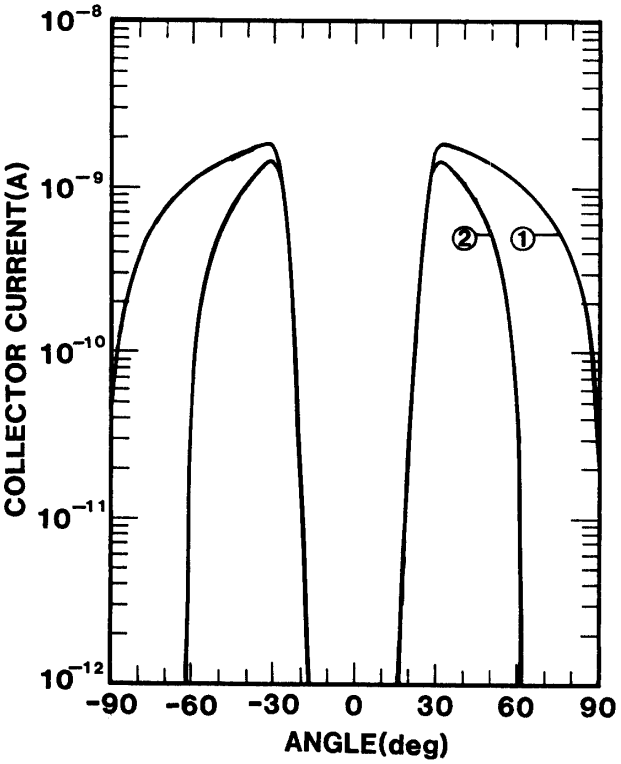

Fig. 4. One of the theoretical ion current versus angle of electrode normal with respect to solar wind stream. Numbers which appear in the figure are the same as for Fig. 3. N_0=5 ions/cm^3, V_b=437.2 Km/sec, T_i=10^4 K and V_{G2}=800 V

$$I_{\text{out}}=\sqrt{\alpha/\pi}\cdot N_0\cdot S_0(\theta)e\left\{V_b\xi\int_{-V_b\xi}^{W-V_b\xi}e^{-\alpha t^2}dt+\frac{1}{2\alpha}(e^{-\alpha V_b^2\xi^2}-e^{-\alpha(W-V_b\xi)^2})\right\} \quad (1)$$

where $\alpha=m_i/2kT_i$, $W=\sqrt{2eV_{G2}/m_i}$, $\xi=\cos\theta$, k Boltzmann's constant, e charge of electron, and $S_0(\theta)$ ion collecting surface area which is shown in Fig. 3. One of the theoretical characteristic curve is shown in Fig. 4, where $S_0(\theta)$ for curve (1) is assumed constant and curve (2) takes the angular dependence which is shown in Fig. 3 into account.

2. Structure of the Faraday Cup

To measure the current of the order of 10^{-12} A with proper frequency response is not an easy task under high voltage operation. Special attention about the structure and the materials of the Faraday cup was paid to block the leakage of the high voltage to the preamplifier. The Faraday cup consists of 4 grids and an ion collector. The 1st grid is grounded to the satellite skin. Square wave high voltage is applied to the 2nd grid to modulate the incoming ions. The 3rd grid is grounded again to block the leakage of the high voltage to the ion collector. The 4th grid is biased at -100 V to suppress the photoelectrons which are emitted from the collector. It is noted, however, that secondary photoelectrons which are emitted from the 4th grid are accelerated to the ion collector. The diameter of the collector is 100 mm and the distance between the 1st grid and the collector is 40 mm. The overall transparency of the 4 mesh grids is 24%.

3. Insights which are Derived from the Theory

3.1. Basic characteristic curves

Fig. 5 shows the changing of the characteristic curve when the second grid V_{G2} varies from 500 V to 800 V. As V_{G2} becomes smaller, angle at the maximum current becomes bigger as we can easily tell by the equation $eV_{G2}=1/2\cdot m_i\ (V_b\cos\theta)^2$. Accordingly maximum ion current becomes smaller because collecting area $S\ (\theta)$ decreases as θ increases. The angle at which the current starts to flow increases as the bulk velocity increases and out put signal becomes weaker. In order to know the lower limit of ion density measurement, Fig. 6 is presented. The figure shows that 1 ion/cm^3 gives 2.5×10^{-10} A (This value is still 100 times larger than 2×10^{-12} A which is the noise level of the ac amplifier). Fig. 7 shows the effect of bulk velocity on the characteristic curve. As the bulk velocity increases, satellite must spin further in order to get modulating signal with V_{G2} constant, because V_{G2} which causes modulated ion current is simply expressed by the $V_{G2}=m_i/2e\ (V_b\cos\theta)^2$ and the relation shows that $\cos\theta$ decreases as V_b increases. Finally the paragraph discusses the effect of ion temperature upon the characteristic curve. When $T_i=0$, the ion current suddenly starts to be modulated at the angle where the bulk velocity component normal to the electrode plane is equal to V_{G2}, as we analysed in the appendix. When T_i becomes higher, rounding of the curve near the collector current maximum becomes more remarkable as shown in Fig. 8. This is very understandable if we think that the curve is a combination of many curves which have different bulk velocities according to the Maxwell energy distribution law.

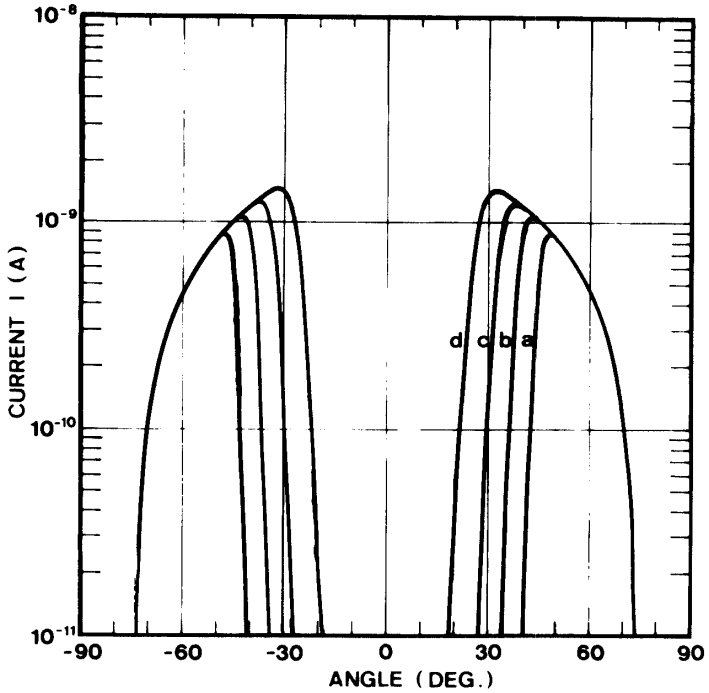

Fig. 5. Changing of the characteristic curve when grid voltage is changed. Grid voltage is changed from 500 V (a), 600 V (b), 700 V (c) to 800 V (d). Back ground parameters are; N_0=5 ions/cm^3, T_i=1.0×10^4 (K) and V_b=1000 V (437.2 Km/sec).

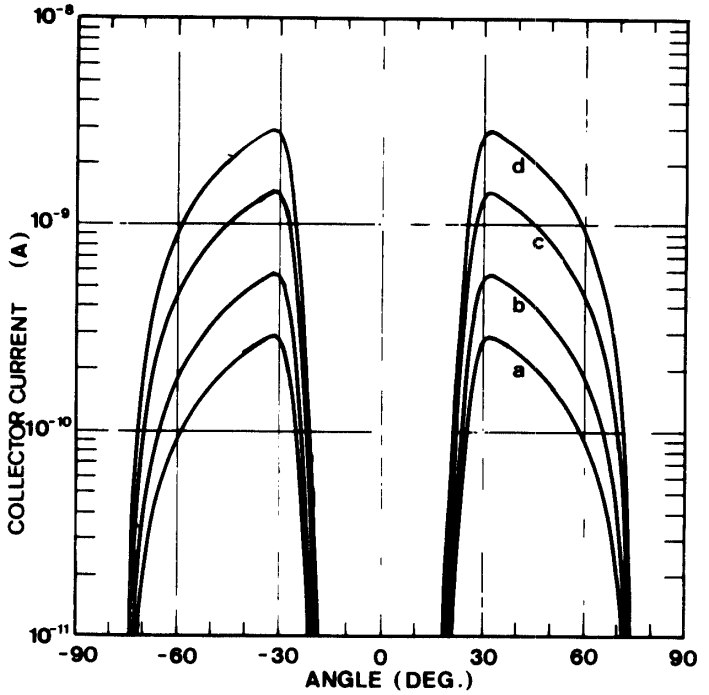

Fig. 6. Increase of ion current when ion density N_0 is increased. 1 ion/cm^3 (a), 2 ions/cm^3 (b), 3 ions/cm^3 (c) and 10 ions/cm^3 (d). V_{G2}=800 V, V_b=1000 eV (437.2 Km/sec), and T_i=1×10^4 K.

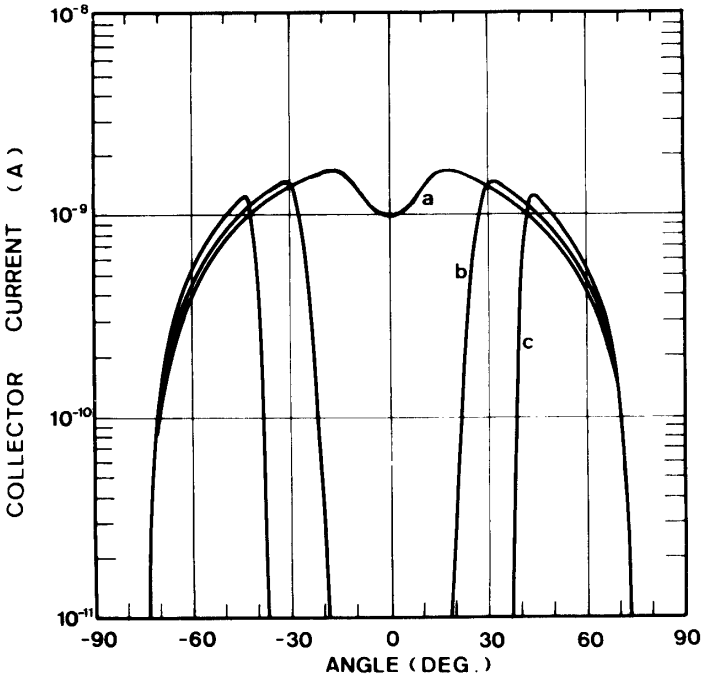

Fig. 7. Changing of the characteristic curve when bulk velocity is changed.
a. V_b=800 V (391.0 Km/sec)
b. V_b=1000 V (437.2 Km/sec)
c. V_b=1400 V (517.3 Km/sec)
V_{G2}=800 V, T_i=1×10⁴ K, and N_0=5 ions/cm³

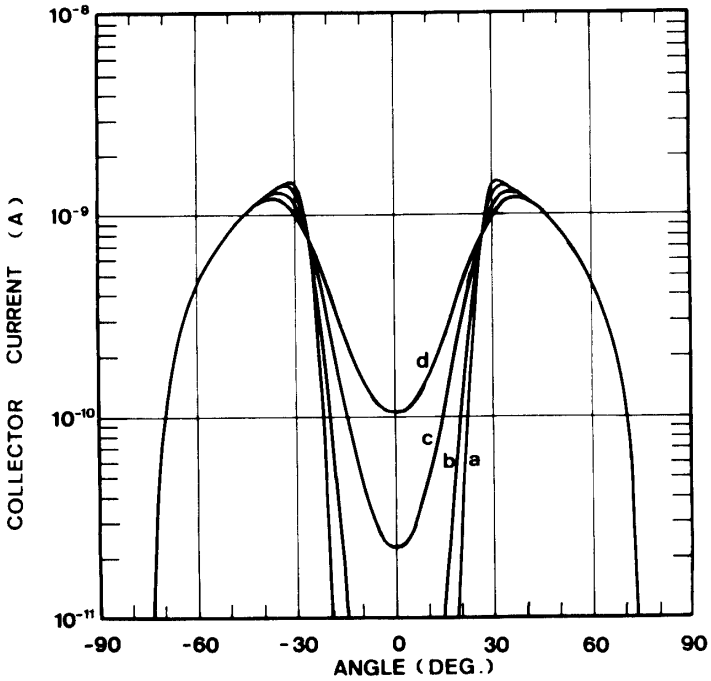

Fig. 8. Effect of ion temperature upon the rounding of the curves near the ion current maximum.
a. T_i=1×10⁴ K
b. T_i=2×10⁴ K
c. T_i=5×10⁴ K
d. T_i=10×10⁴ K
N_0=5 ions/cm³, and V_b=1000 eV (437.2 Km/sec)

3.2. Error-generating factors

One of the biggest factors which influence the accuracy of the measurement is a quality of the high voltage which should be applied to the second grid. Especially fluctuation of the amplitude and wave shape of the high voltage influences the accuracy of the measurement of ion temperature. As Fig. 9 shows, the wave shape of the high voltage is not ideal as we used in order to derive the equation (1). After the sudden rise up of the square wave voltage, the wave still continues to grow with a small slope and the potential difference of 20 V exists between the first and the final value. The effect of the wave shape upon the parameters to be obtained by curve fitting is studied by investigating the curves which are calculated with slightly different V_{G2}. Three pairs of Faraday cup characteristic curves are shown in Fig. 10 with three different bulk

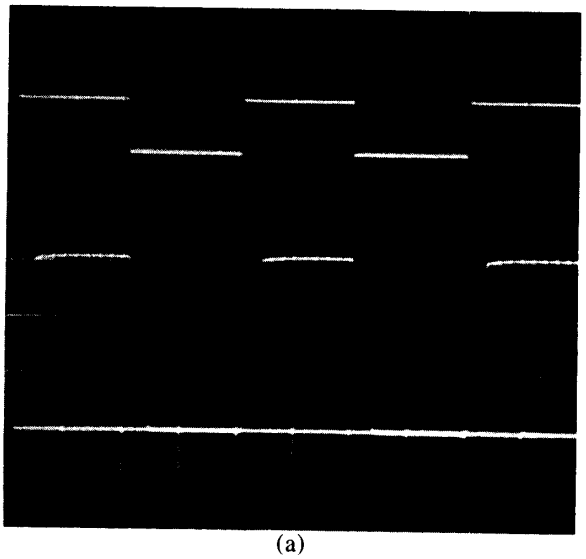

(a)

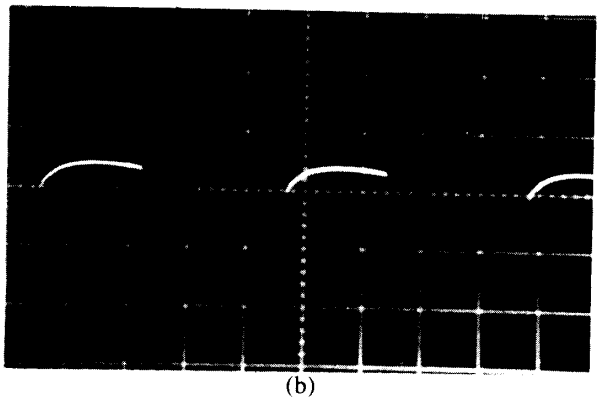

(b)

Fig. 9. a. Wave shape of the high voltage (lower column). The flat part of the high voltage of the figure is magnified in Fig. 9.b in order to see the small distortion of the high voltage. (Vertical axis, 500 V/div, horizontal axis 0.5 msec/div). Upper column is the synchronizing pulse.

b. Magnified flat part of the high voltage shown in Fig. 9.a. (Vertical axis; 50 V/div, horizontal axis; 0.5 msec/div.).

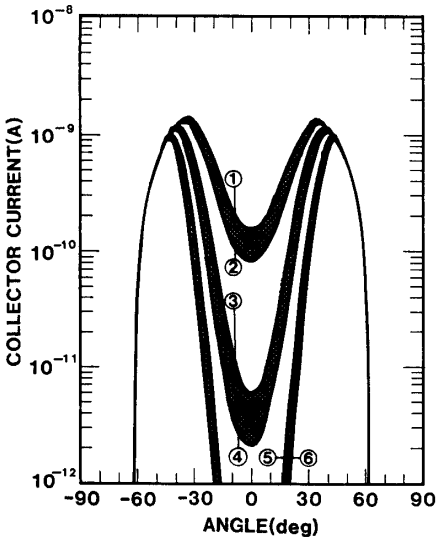

Fig. 10. Three pairs of theoretical curves which are calculated with V_{G2}=960 V and 1000 V, N_0=5 ions/cm^3 and T_i=10^5 K.
curves (1) and (2); V_b=1200 V
curves (3) and (4); V_b=1400 V
curves (5) and (6); V_b=1600 V

velocities. A pair of the curves are calculated with V_{G2}=1000 V and 960 V and are connected with gray shade. The figure shows that when the high voltage has 40 V fluctuation, the curve fluctuates between (1) and (2) ((3) and (4), and (5) and (6)).

As the bulk velocity decreases (478.9 km) the difference of the two characteristic curves for V_{G2}=1000 V and 960 V becomes bigger. We evaluate the effect by fitting the curve (1) which is originally calculated at V_{G2}=1000 V to theoretical curve by assuming V_{G2}=960 V and get another V_b, T_i and N_0. The rests are also tested in the same way. The results are summarized in Fig. 11. The conclusions which are derived from Fig. 11 are; (1) Ion density is more accurately determined when ion temperature is low (T_i=10000 K). This is reasonable because ion density is obtained from the curve near the peak current and rounding of the curve near the peak is less remarkable than for high temperature. (2) Measurement accuracy of the bulk velocity does not vary very much by the ion temperature because the ion temperature contributes only to the rounding of the curve near the current maximum, but not the angle at the current maximum. (3) Measurement of ion temperature is especially degraded as the ion temperature decreases (T_i=10000 K) and the tendency is more remarkable when bulk velocity is low (eg. V_b=1200 eV).

The discussion which was done in the above is also applied to the time variation of the amplitude (drift) of high voltage. That is, in other word, if we want the measurements of three parameters within 10% error, stability of V_{G2} should be ±0.4%.

One more factors to be discussed in terms of high voltage is the biased level of V_{G2}. High voltage generator which was designed and actually manufactured changes its amplitude from ≈30 V to 1~1.7 KeV in stead of from 0 V. In order to see the effect of the biased voltage, we calculate the eq. 1 for the small V_{G2}, which is shown in Fig. 12. The influence of the biased level upon the characteristic curve is finally studied by calculating I_{out} (V_{G2}=1~1.7 KeV)-I_{out} (V_{G2}=60~300 V) for the same bulk velocity and T_i. Accordig to the figure, maximum collector current which flows when V_{G2}=100 V is 10^{-11} A and this value is 1/40 of the maximum collector current at V_{G2}=300 V in the density of 5 ions/cm^3. Therefore we can conclude that the biased level of the high

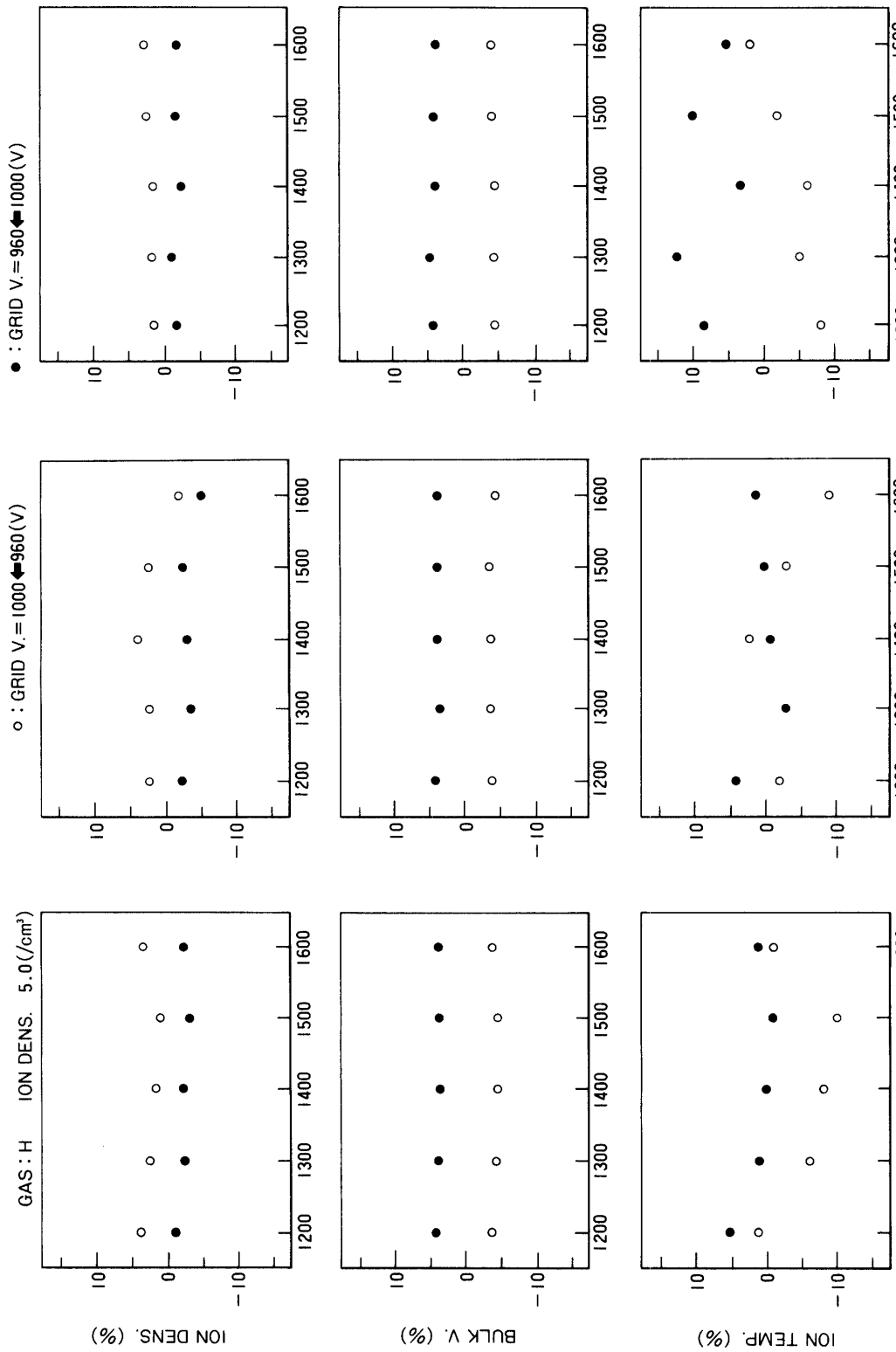

Fig. 11. Ambiguity of N_0, V_b and T_i measurements when distortion of the flat part of the high voltage which was shown in Fig. 9.b is 40 V.

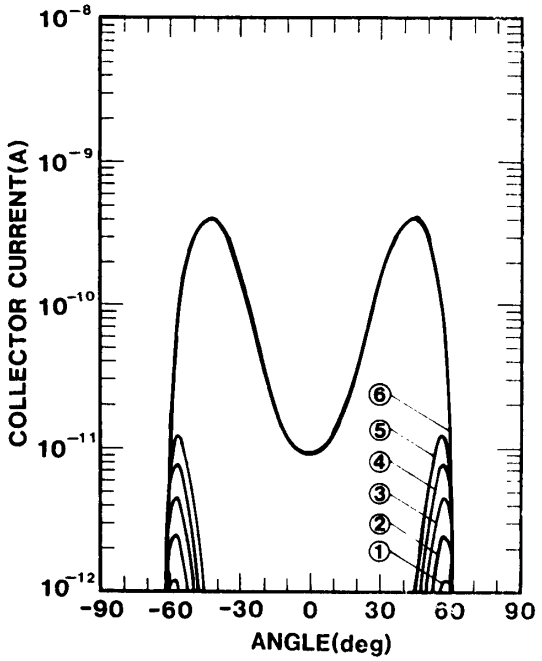

Fig. 12. Characteristic curves when the amplitude of high voltage has (1) 60 V, (2) 70 V, (3) 80 V, (4) 90 V, (5) 100 V and (6) 300 V for $T_i=10^5$ K, $V_b=309.1$ Km/sec and $N_0=5$ ions/cm^3.

voltage does not practically give a serious influence on the accuracy of the solar wind measurement.

3.3 Curve fitting

The first step to find final value of N_0 and V_b is to find the rough initial value. The initial value is roughly obtained by utilizing the equation described below (maximum current method)

$$V_b=\sqrt{2eV_{G_2}/m_i\cos^2\theta_{\max}} \tag{2}$$

$$N_0=i_{\max}/eV_b\cdot\cos\theta_{\max}\cdot S_0(\theta_{\max}) \tag{3}$$

where $\theta_{\max}$ is the angle where ion current becomes maximum. N_0 and V_b which are thus obtained are given to eq. (1) as a initial condition. Initial value of T_i is set to $T_i=10000$ K. As shown in Fig. 13, curve (1) is the theoretical curve where the rough V_b and N_0 are included and then the curve (2) was obtained in order to minimize the standard deviation C_0 by changing N_0 at each angles where data were taken.

$$C_0=\sum_{-90^\circ}^{90^\circ}\{(V_b-V_{b0b})^2+(N_0-N_{0b})^2+(T_i-T_{0b})^2\}\,, \tag{4}$$

where T_i is still unchanged.

After N_0 is roughly adjusted, V_b is started to be changed so that C_0 again becomes

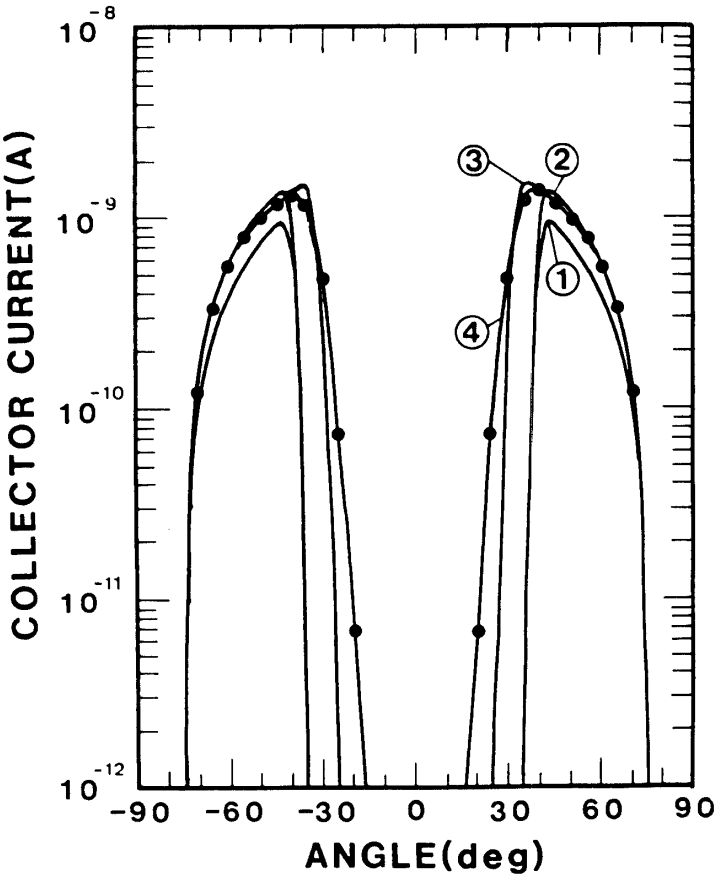

Fig. 13. Process of curve fitting. The bulk velocity which was given by V_b=1400 eV is 517.3 Km/sec. V_{G2} is 1000 V.

	N_i/cm^3	V_b Km/sec (eV)	T_i (K)	ST·DE×10^{-12} A
(1)	3.4	570 (1700)	10000	417.58
(2)	4.9	570 (1700)	10000	372.46
(3)	4.9	517.3 (1400)	10000	96.4
(4)	5.0	517.3 (1400)	40000	0.15

minimum. The same process is repeated for T_i and finally curve 4 is obtained. Although the curve fitting described above was found to work nicely, one disadvantage of the fitting is a long computing time. When we take one data sample for every one degree, even M300 FACOM computer needs one minutes. Since S3300 computer whose computing time is slower than M300 which is currently working is planned to be used for real time data processing for MS-T5 experiment, the long computing time is a problem. As the computing time depends on the number of data points to be put in the computer, we tried to estimate the computing time by decreasing the number of data points. As shown in Fig. 14, cumputing time for curve fitting decreases as the sampled data become less. For example, if we sample one data every 10 degrees, the computing time is about 30 sec, still keeping 1% error. Black circles shows the measurement accuracy of the data obtained by using maximum current method. The accuracy of the data processing by means of the simple method could be within 20%, which might be still good for quick

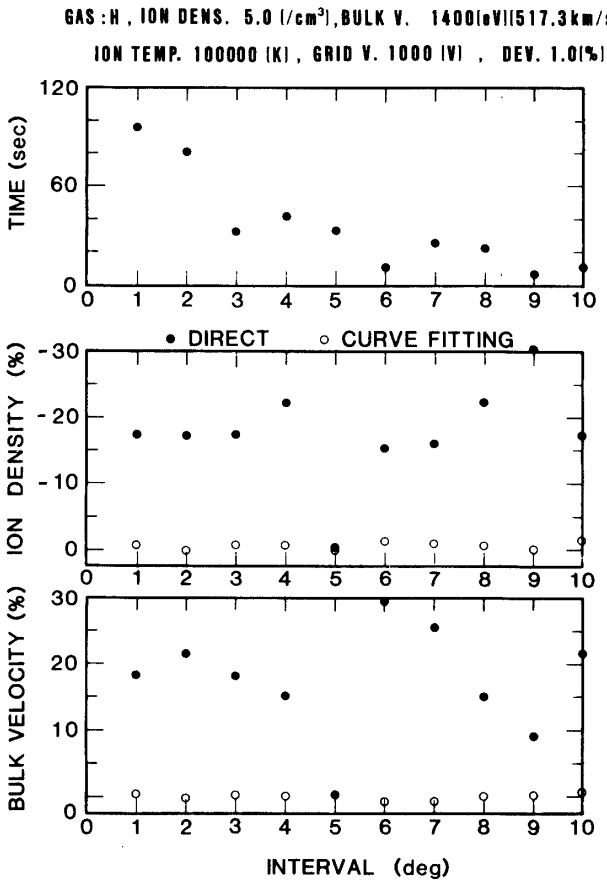

Fig. 14. Computing time when sample interval is changed. Plasma parameters are N_0(H)=5.0 ions/cm^3, V_b=1400 eV (517.3 Km/sec), and T_i=10^5 K respectively. The 2nd grid voltage is V_{G2}=1000 V. ●mark was obtained from simple method. ○mark was from the curve fitting.

look data analysis. In order to see the effect of ion temperature T_i upon the accuracy of the derivation of the parameters, V_b and N_0, Fig. 15 is presented. The figure shows that V_b and N_0 can be calculated within 15% error for an average ion temperature of 5×10^4 K.

4. Laboratory Experiment

Laboratory experiment was carried out in order to study the collector ion current/spin angle characteristics.

He ion beam of 40 cm diameter was generated by cylindrical dc plasma source and ions were subtracted through two grid mesh planes which are located at one side of the plasma generator. Plasma generator was floated and voltage V_B was applied between the plasma generator and the ground. Ion beam energy was freely controlled by changing V_B. Plasma density N_0 is controlled either by heater current of plasma generator or by the discharge current. Helium gas was continuously injected with back ground initial pressure of 10^{-5} Torr and the pressure inside the chamber was kept constant at 10^{-4} Torr during the experiment. Faraday cup is set up in the center of the plasma chamber and the

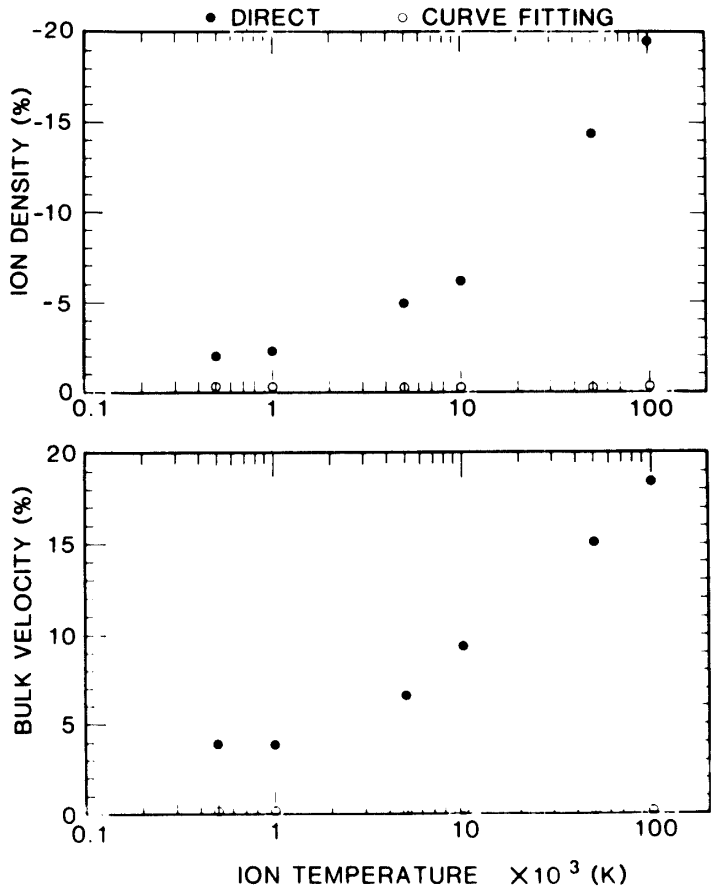

Fig. 15. Dependence of ion temperature upon the curve fitting accuracy. Black circles are the number obtained by a simple method (maximum current method). The values at vertical axis show the deviation from true value. Parameter are N_0=5.01 ions/cm^3 and V_b=517.3 Km/sec respectively. The second grid voltage is V_{G2}=1000 V.

cup is rotated with respect to the ion flow from the outside of chamber so that the rotation simulates a spacecraft spinning. Ac ion current is recorded by means of a chart recorder as the Faraday cup is rotated. At the back of the Faraday cup, circular electrode of 40 cm diameter was installed in order to calibrate the Faraday cup. The ion current i which flows into the circular electrode gives the ion density by the following simple equation

$$N_0 = i/S_0 \cdot e \cdot \sqrt{2eV_B/m_{He}} \tag{5}$$

where m_{He} helium ion mass, e electronic charge, and S the surface area of the circular electrode. By comparing the ion densities which were obtained from the circular electrode and from Faraday cup, we can evaluate and confirm the transmission of the Faraday cup which has been estimated as 24%. Fig. 17a shows an example of characteristic curve which are thus obtained. White circles show the experimental data. Fitting of the characteristic curve described by eq. (1) to the experimental data is repeated until the error C_0 in eq. (4) becomes minimum. T_i, V_0 and N_0 which are finaly

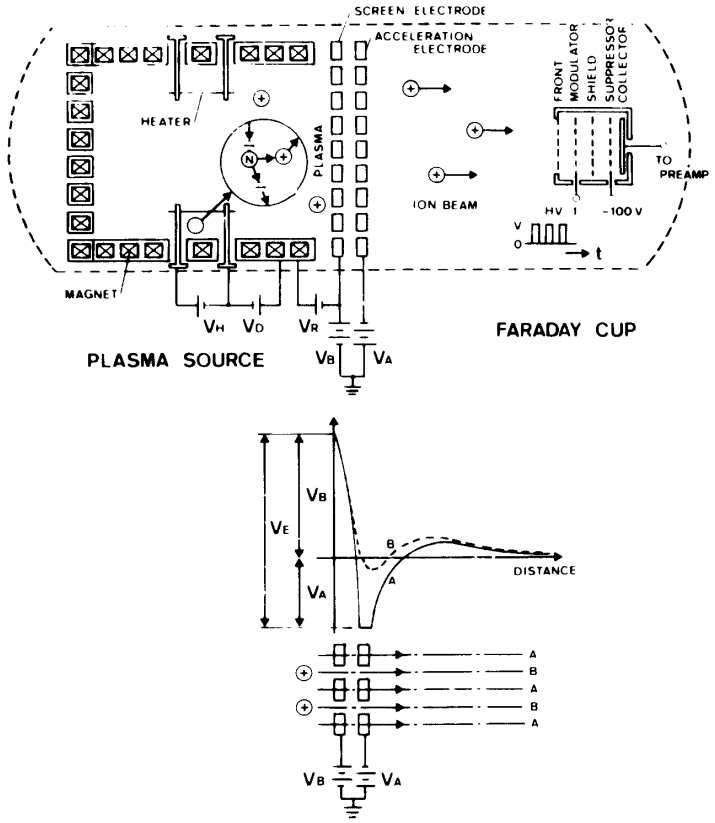

Fig. 16. Experiment set up and ion source.

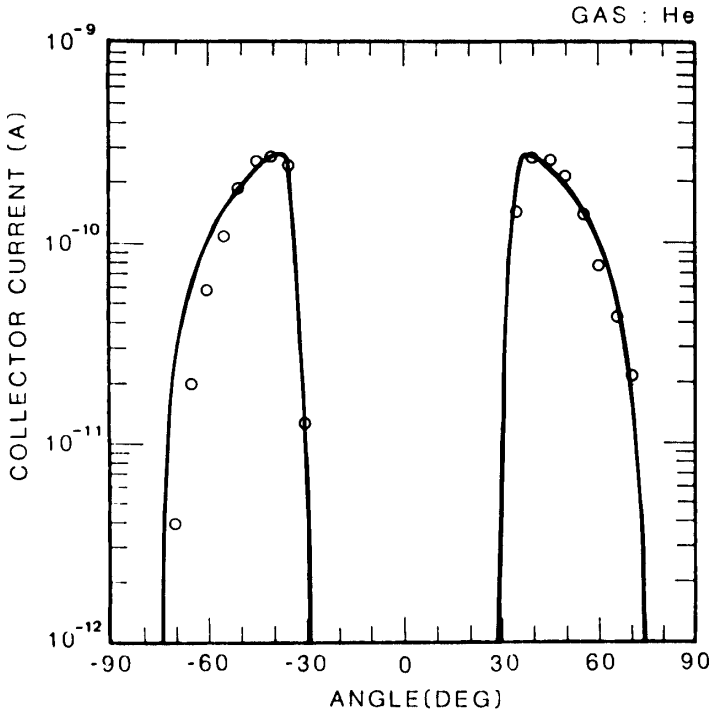

Fig. 17. Curve fitting of the theory with measured characteristic curve. N_0, V_b and T_i which are obtained from curve fitting to the measured curve are 2.25 ions/cm^3, 172.1 Km/sec and 4000 K espectively. While bulk velocity which was given by V_B=800 V is 195.5 Km/sec. The 2nd grid voltage is 500 V.

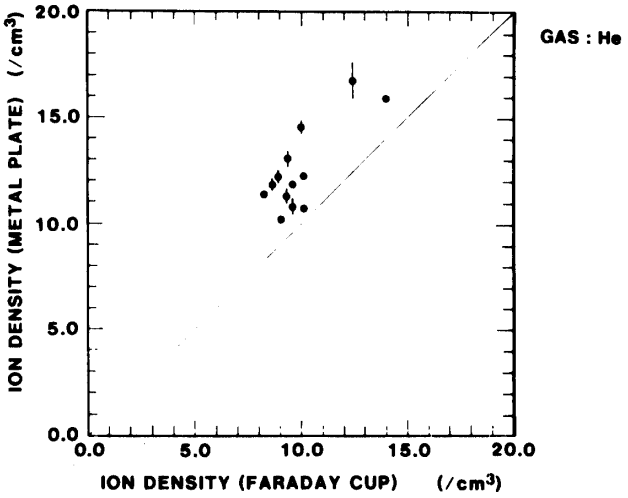

Fig. 18. a. Comparison of H_e ion densities which were obtained from curve fitting and which were measured by a big electrode located at the rear of Faraday cup.

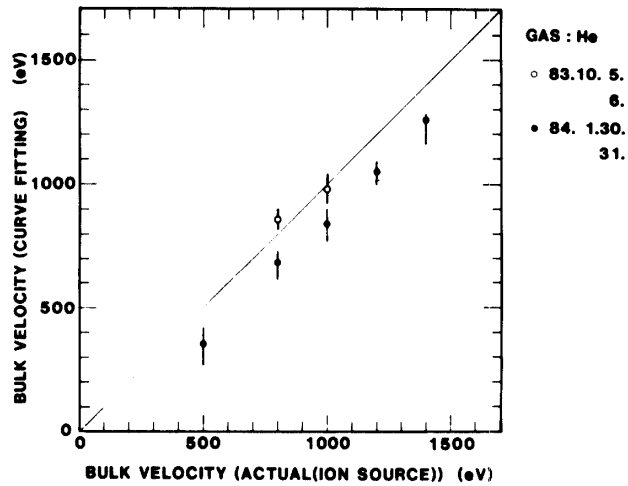

Fig. 18. b. Comparison of bulk velocity of H_e ions, V_b which was obtained from curve fitting and generated by plasma source. White circles were obtained on the 5th and 6th, December 1983 when electrodes of Faraday cup are comparatively clean.

obtained are 2.35 ions/cm^3, 209.7 Km/sec and 8000 K. While plasma bulk velocity which was set by V_B is 1 KeV (218.6 Km/sec). The agreement is within 5%. The ion density is very reasonable as we will describe later. Although we do not have any way to check T_i inside plasma generator as well as in the test plasma region, the T_i is considered to be $\approx$10000 K. The measurements which are obtained by curve fitting are surmmarized in Fig. 18a and 18b. The Figure 18a shows the comparison of N_0, which are obtained by Faraday cup and metal electrode. In the worst case N_0 is evaluated 30% lower than the metal electrode data. We finally know that the deviation is caused by the contamination of the Faraday cup. Fig. 18b shows the bulk velocities which were set by an ion accelerating voltage V_B of plasma generator and the results obtained by curve fitting. White circles show the good agreement within the accuracy of 5%. On the other hand,

for the black circles, measured bulk velocities are rather lower than the true value whose error is much bigger than we expected from the computer simulation. This deviation can be phenomenologically explained by taking into account the electrode contamination.

5. Electrode Contamination

As we mentioned in the previous paragraph, the bulk velocity which is obtained by curve fitting is lower than the value which is expected. As shown in Fig. 19, white circles shows the characteristic curve which are obtained when V_{G2} was 600 V and bulk velocity V_b=800 V respectively. However when we theoretically compute the characteristic curve by putting V_{G2}=600 V and V_b=800 V to the equation (1), curve (1) in the Fig. 19 is generated, which does not fit the observed characteristic curve. However when V_{G2} is set at V_{G2}=690 V instead of V_{G2}=600 V in the equation (1) the theoretical curve fits very well the observed characteristic curve. This seems to suggest that the 2nd grid voltage is effectively higher than the voltage which is really applied. We can conclude that the phenomenon is caused by the positive charging of the electrode, that is, incoming ions stick to the surface of the electrode.

In order to see this phenomenon in more detail, Faraday cup was faced toward ion stream. Bulk velocity was set by the accelerating voltage V_B which is shown in Fig. 16. V_{G2} of the Faraday cup was gradually increased and the collector current was monitored. If the instrument works fine, ion flux should not be modulated when the V_{G2} is lower than

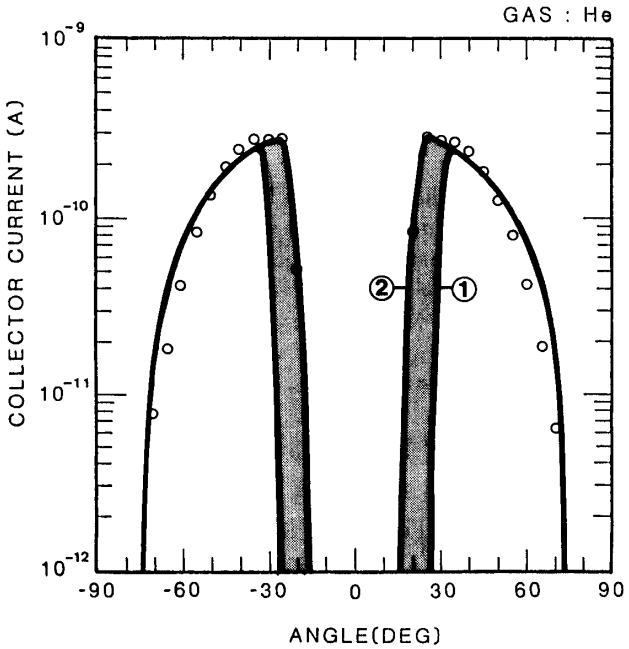

Fig. 19. Shift of the characteristic curve which is caused by the electrode charge-up.
curve 1; V_b=800 eV and V_{G2}=600 V
curve 2; V_{G2} was changed to 690 V in order to fit the measured curve by assuming that the electrode is charged up to 690 V in addition to 600 V.
N_0=2 ions/cm^3, V_b=800 eV and T_i=3000 K.

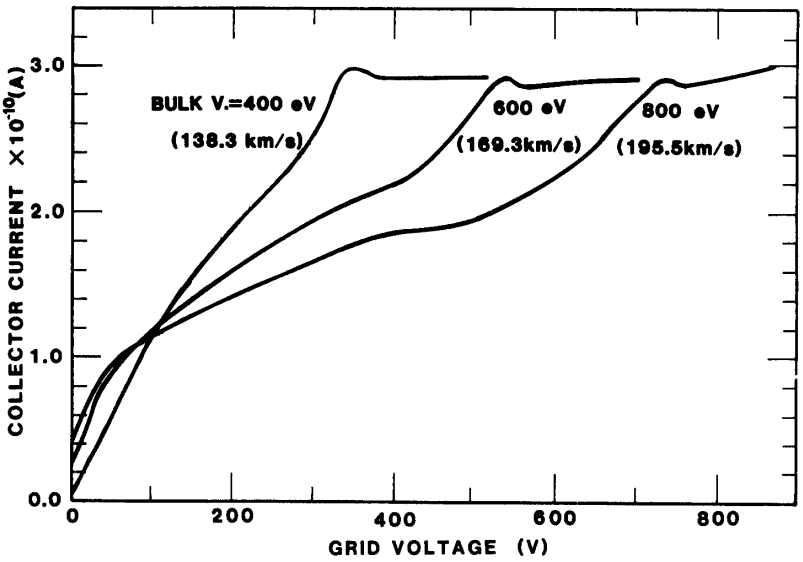

Fig. 20. Ion collector current versus the 2nd grid voltage when electrode faces the plasma flow which were taken just after the evacuation of the chamber started.

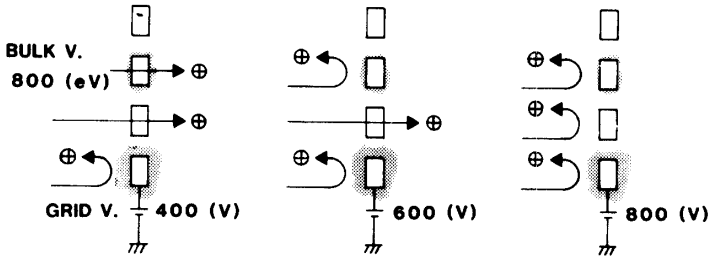

Fig. 21. Model of electrode contamination.

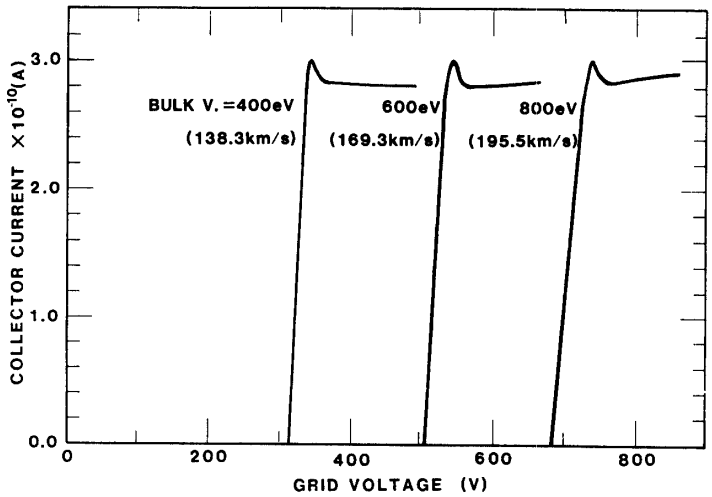

Fig. 22. The same as for Fig. 20 except the data were taken after 3 days of vacuuming.

ion beam energy. However as Fig. 20 shows, collector signal already appears at V_{G2} which is far below the ion bulk energy. This mysterious phenomenon is explained by the model described in Fig. 21. When the grid voltage is e.g. 400 V, some part of the contaminated electrode charges up and get higher voltage. Since the degree of charging up might be different at various parts of the electrode surface, potential of the electrodes varies depending on the places of the electrode. As the voltage of the electrode is increased (e.g. 800 V), all part of the electrode surface finally becomes more than 800 V, which repel all the ions. This explain the final part of the curves which are shown in Fig. 17. In fact, when the Faraday cup is vacuumed for two days and electrode becomes cleaner, the phenomenon decreases as shown in Fig. 22. The data which were plotted in the Fig. 19 can thus be explained by the idea of electrode contamination.

6. Flight Model of Solar Wind Measurement

6.1. *Block diagram*

Block diagram of the instrument is shown in Fig. 24. Square wave of the frequency 400 Hz is applied to the 2nd grid (1.25 msec on and 1.25 msec off). The amplitude of the high voltage can be changed depending on the solar wind velocity from the earth. The amplitude changing has 3 modes. They are;

(1) Fixed bias mode; to fix the high voltage at one constant voltage during the observation. The mode will be used during most of the mission.

(2) Sweep voltage mode; to increase the high voltage stepwisely every 1~2 spins in high bit rate. For low bit rate, high voltage is kept constant while 1 or 2 spin data are read out. High voltage is increased from 70 V and finally goes to 1.85 KV (maximum) and again back to 70 V.

(3) Fine sweep bias mode; to begin the gradual step up of the high voltage from the initially controlled voltage with smaller step.

Modulated ion current which is generated according to the principle described in paragraph 1 is detected by means of a dc amplifier and only 400 Hz ac current is magnified by lock-in amplifier, detected and finally digitized. Secondary photoelectron current which is $\sim 10^2$ times higher than the modulated ion currents are again amplified

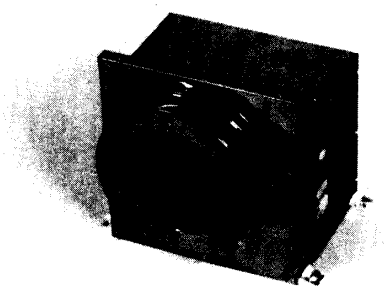

Fig. 23. Photograph of the Flight model on board MS-T5.

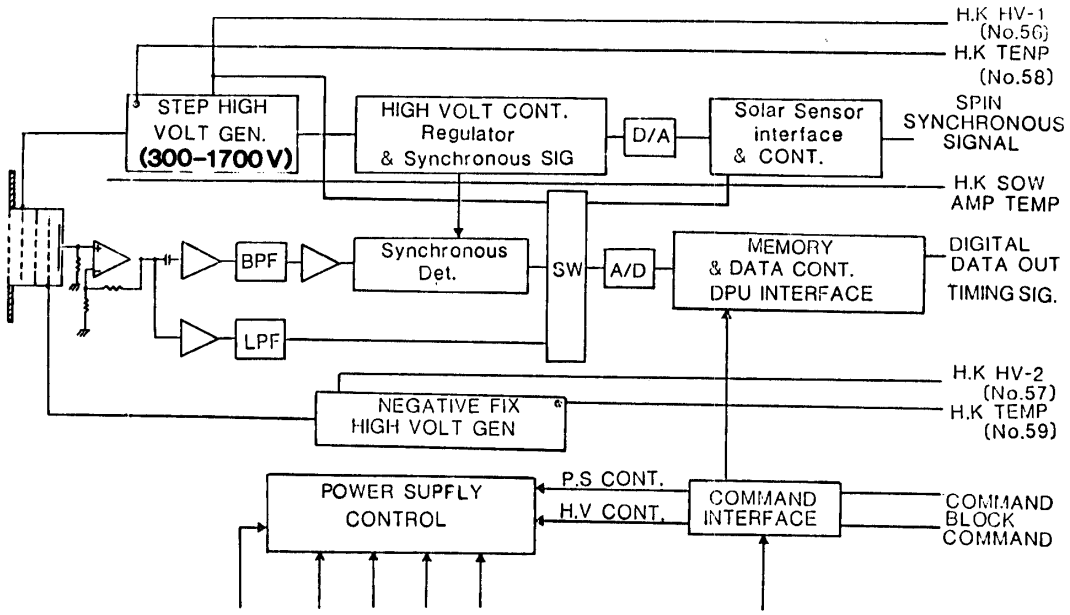

Fig. 24. Block diagram of the experiment. 2 preamplifiers which are not shown here are installed for redundancy.

by another amplifier. The dc currents (secondary electron current including modulated ion current) which vary during one satellite spinning is used to check the angular characteristic of the Faraday cup itself which has already been tested in the laboratory plasma as well as by the computer calculation as shown in Fig. 3. Minimum input-reduced ac current which can be detected by the preamplifier is 2×10^{-12} A. However the leakage of the high voltage to the collector raises the noise level of the amplifier. The noise level corresponds to the current of 2×10^{-11} A when the 2nd grid voltage becomes 1.85 KV. The gain of both ac and dc amplifiers can be changed depending on the plasma density. The ac amplifier has further option that the gain can be automatically changed every spin in high bit rate telemetry mode. In low bit telemetry mode (16 sec/1 frame) the gain is kept constant until one spin data is read out (48 sec or 64 sec). Frequency response of the overall system is 40 Hz. The instrument operation items which are controlled by the commanding from the earth are;

1. Setting of gains of ac/dc amplifiers.
2. Choosing gain control mode; fixed gain/gain alternating.
3. Setting the high voltage application either at the stepwise increase or at the fixed voltage.
4. Choosing one of the two dc amplifiers A or B.
5. Calibration of the overall amplifier.

6.2. *Data sampling and Telemetry format*

Modulated ion current is sampled between $-90°$ and $+90°$ with respect to the sun-satellite direction. Although the sensor sensitivity to the solar wind ions is limited from $-60°$ to $60°$ as described in the previous paragraph, we expect that some Halley comet-related plasma stream might be detected beyond $\pm60°$. During the mission, most

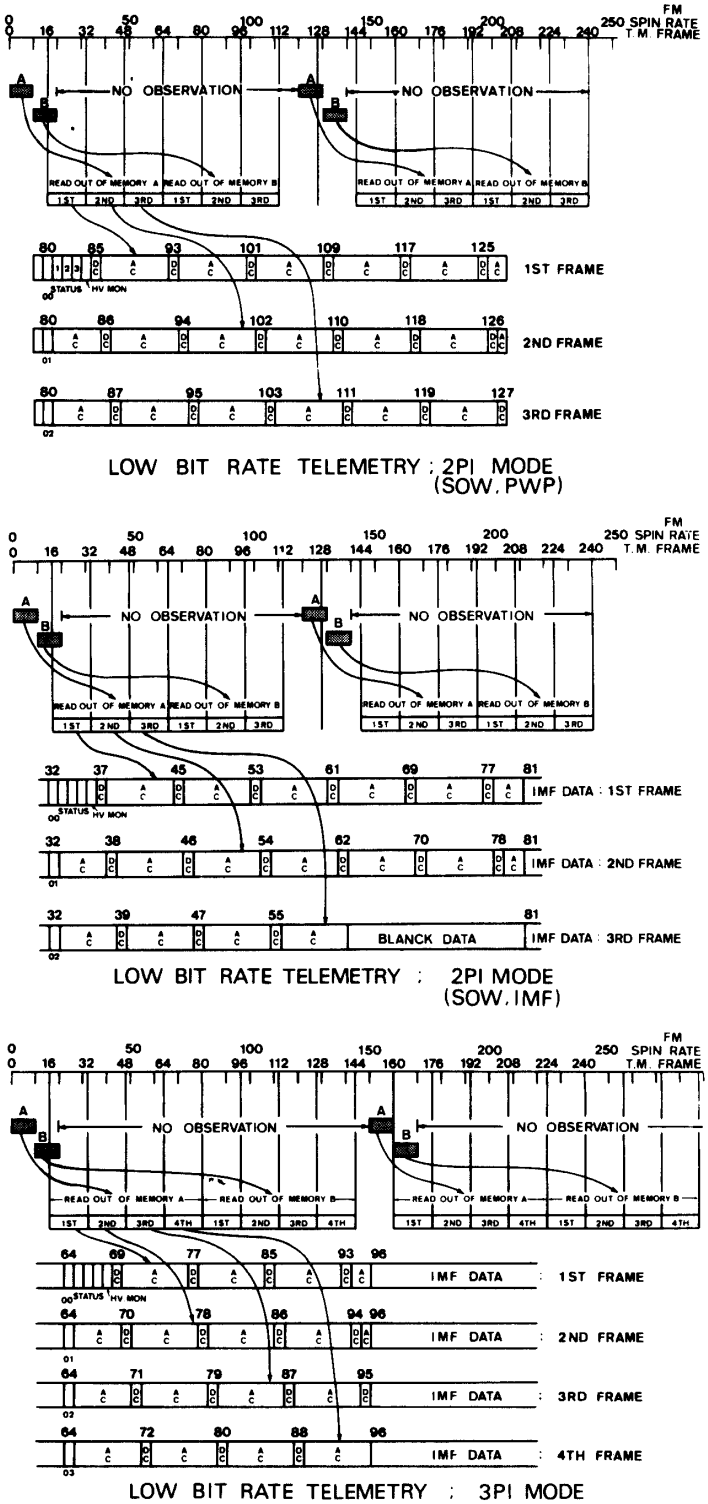

Fig. 25. An example of the low bit rate telemetry format. Data read-out is synchronized with satellite spin.

experiments are operated in low bit rate telemetry mode (64 bits/sec). 128 data points are sampled while the spacecraft spins from $-90°$ to $+90°$ with respect to sun-satellite line. This means the angular resolution of the Faraday cup is 180/125 degree. Data are stored in memory A until one spin sampling is completed. As soon as the memory A completes one spin data sampling, the memory A starts to send the data to telemetry system. As soon as the memory A starts to send out the data, memory B starts sampling for one spin observation. Next observation is not possible until memory B finishes the sample data sending. When all three experiments (solar wind plasma, plasma wave and interplanetary magnetic field) are switched on (3 PI mode), 128 points which are sampled during one satellite spin are distributed to 4 frames telemetry format. This means that 64 sec are needed for the data telemetry. When two experiments among the three are switched on, 48 sec are needed to telemeter the one spin data.

When the automatic amplifier gain is commanded from the ground, the gain is alternatively changed; the amplifier gain is kept low (or high) during 64 sec (48 sec) which corresponds to 4 (3) frames and for another 64 sec/48 sec, the amplifier gain is kept highlow.

When sweep voltage mode is chosen in automatic amplifier gain, the voltage is kept constant during 128 sec (64 sec) which correspond to 8 (6) frames and for the next 128 sec (64) the voltage is kept at another amplitude and so on. That is, the high voltage is kept constant until alternative H/L gain switching completes. For high bit rate operation (which might not be so often operated in a long distance from the earth), data are sampled at much faster rate (48 words/32 words/Frame).

Acknowledgements

One of the authors (K.I. Oyama) expresses his sincere thanks to Professor H. Oya who gave him a ring from Tohoku University to install a Faraday cup in the satellite MS-T5. K. Nakazawa is indebted to Mr. W. Miyake for his advises in computer programming. The authors are very grateful to Messrs. Abe, Shomura, Kokubo, Sima and Koga of Meisei Electric Company Ltd. for the designing and manufacturing of the electronics and the sensor itself.

Appendix A. Derivation of Equation 1

We take coordinate system as follows; Z-axis is vertical to the collector plane of the Faraday cup. X-axis is perpendicular to the Z-axis in the plane including Z-axis and the direction of the solar wind. Y-axis is perpendicular to both X- and Z-axis. If we assume that the angle between V_b and Z is Θ, we have,

$$\vec{V}_b = V_b \begin{pmatrix} \sin\Theta \\ 0 \\ \cos\Theta \end{pmatrix} \equiv \begin{pmatrix} v_{x0} \\ 0 \\ v_{z0} \end{pmatrix} \tag{A1}$$

and the distribution can be written as

$$f(v_x, v_y, v_z)=\tilde{A}\exp\left[-\alpha\{(v_x-v_{x0})^2+v_y^2+(v_z-v_{z0})^2\}\right] \tag{A2}$$

where

$$\alpha=m_i/2kT_i \quad \text{and} \quad \tilde{A}=(\alpha/\pi)^{3/2}\cdot N_0$$

The number of particles (N) which have energy greater than W is expressed as,

$$N=\int_{-\infty}^{\infty} dv_x \int_{-\infty}^{\infty} dv_y \int_{W}^{\infty} dv_z f(\vec{V})\cdot v_z \cdot S_0(\theta) \tag{A3}$$

where $W=\sqrt{2eV_{G2}/m_i}$ and S_0 is the area of the aperture. Since the Faraday cup are designed to detect the ion fluxes when retarding voltages are alternately repeated between V_{G2} volts and 0 volt, the ion flux can be written as,

$$N_{\text{out}}=\int_{-\infty}^{\infty} dv_x \int_{-\infty}^{\infty} dv_y \int_{0}^{W} dv_z f(\vec{V})\cdot v_z \cdot S_0(\theta) \tag{A4}$$

Putting eq. (A1) into the above equation makes,

$$N_{\text{out}}=\int_{-\infty}^{\infty} dv_x \int_{-\infty}^{\infty} dv_y \int_{0}^{W} dv_z \tilde{A}\exp\left[-\alpha\{(v_x-v_{x0})^2+v_y^2+(v_z-v_{z0})^2\}\right]\cdot v_z \cdot S_0(\theta) \tag{A5}$$

Generally in the above equation, S_0 is not constant but depends on θ which is expressed as

$$\theta=\tan^{-1}(\sqrt{v_x^2+v_y^2}/v_z)\equiv\tan^{-1}(v_\perp/v_z) \tag{A6}$$

Physical meaning of the angle dependence of the surface area is clear from the fact that not all particles, which pass through the entrance with the same velocity V_i, can reach the collector. Some part of them collides with the wall of the Faraday cup and can not reach the collector, but some other can reach the collector. As the dependence of S_0 on θ can be easily calculated, final expression of the ion flux is written as follows; The configuration of the Faraday cup is shown in Fig. A-1. Several parameters which are shown in the Fig. A-1 are introduced as

$$X_s=HI\times\frac{v_\perp}{v_z}$$

$$X_L=(HI+HO)\times\frac{v_\perp}{v_z}-(R_L-R_s)$$

$$X_A=(2R_s+X_s)/2$$

$$X_B=\{2(R_LX_L-R_sX_s)+(X_L^2-X_s^2)\}/2(R_L+X_L-R_s-X_s)$$

$$X_C=(2R_LX_L+X_L^2)/2(R_L+X_L-R_s)$$

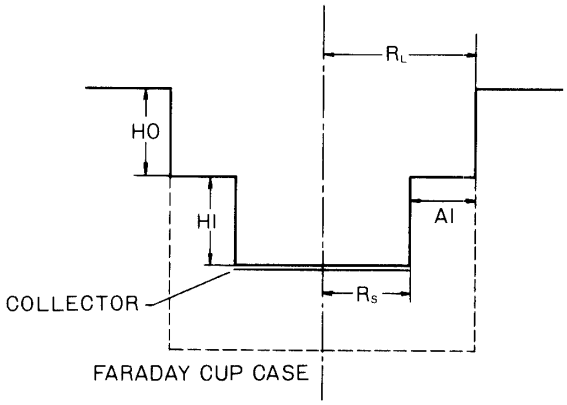

Fig. A1. Dimension of Faraday cup which is used in the experiment.

in which, all of X_s, X_L, X_A, X_B and X_c are the function of v_z and $v_\perp$.

Effective entrance area depends on $\tan^{-1}(v_\perp/v_z)$, which is written as

$$S_1(v_z, v_\perp)=2R_s\left\{\cos^{-1}\left(\frac{X_A-R_s}{R_s}\right)-\frac{X_A-R_s}{R_s}\sqrt{1-\left(\frac{X_A-R_s}{R_s}\right)^2}\right\}$$

$$\text{for}\quad 0<\frac{v_\perp}{v_z}<\frac{R_L-R_s}{HO}$$

$$S_2(v_z, v_\perp)=R_L^2\left\{\cos^{-1}\frac{R_L+X_L-X_B}{R_L}-\frac{R_L+X_L-X_B}{R_L}\sqrt{1-\left(\frac{R_L+X_L-X_B}{R_L}\right)^2}\right\}$$
$$+R_s^2\left\{\cos^{-1}\frac{R_s+X_s-X_A}{R_s}-\frac{R_s+X_s-X_A}{R_s}\sqrt{1-\left(\frac{R_s+X_s-X_A}{R_s}\right)^2}\right.$$
$$\left.-\cos^{-1}\frac{R_s+X_s-X_B}{R_s}+\frac{R_s+X_s-X_B}{R_s}\sqrt{1-\left(\frac{R_s+X_s-X_B}{R_s}\right)^2}\right\}$$
$$+R_s^2\left\{\cos^{-1}\frac{X_A-R_s}{R_s}-\frac{X_A-R_s}{R_s}\sqrt{1-\left(\frac{X_A-R_s}{R_s}\right)^2}\right\}$$

$$\text{for}\quad \frac{R_L-R_s}{HO}\leqq\frac{v_\perp}{v_z}<B$$

$$S_3(v_z, v_\perp)=R_L^2\left\{\cos^{-1}\frac{R_L+X_L-X_C}{R_L}-\frac{R_L+X_L-X_C}{R_L}\sqrt{1-\left(\frac{R_L+X_L-X_C}{R_L}\right)^2}\right\}$$
$$+R_s^2\left\{\cos^{-1}\frac{X_C-R_s}{R_s}-\frac{X_C-R_s}{R_s}\sqrt{1-\left(\frac{X_C-R_s}{R_s}\right)^2}\right\}$$

$$\text{for}\quad B\leqq\frac{v_\perp}{v_z}<\frac{R_L+R_s}{HI+HO}$$

where B is the solution of $v_\perp/v_z$ for $X_A=X_B$.

Then, the final expression of ion flux is written as

$$
\begin{aligned}
N_{\text{out}} = \tilde{A} \int_0^W dv_z \int_0^{(R_L-R_s)/HO} v_\perp dv_\perp \int_0^{2\pi} d\psi \times S_1(v_z, v_\perp) \\
\times \exp\left[-\alpha\{(v_\perp \cos\psi - v_{x0})^2 + v_\perp^2 \sin^2\psi + (v_z - v_{z0})^2\}\right] \\
+ \tilde{A} \int_0^W dv_z \int_{(R_L-R_s)/HO}^B v_\perp dv_\perp \int_0^{2\pi} d\psi \times S_2(v_z, v_\perp) \\
\times \exp\left[-\alpha\{(v_\perp \cos\psi - v_{x0})^2 + v_\perp^2 \sin^2\psi + (v_z - v_{z0})^2\}\right] \\
+ \tilde{A} \int_0^W dv_z \int_B^{(R_L+R_s)/(HI+HO)} v_\perp dv_\perp \int_0^{2\pi} d\psi \times S_3(v_z, v_\perp) \\
\times \exp\left[-\alpha\{(v_\perp \cos\psi - v_{x0})^2 + v_\perp^2 \sin^2\psi + (v_z - v_{z0})^2\}\right]
\end{aligned}
\tag{A7}
$$

Since the integral has a complicated form, accurate analysis needs computer calculations. However, in case that the detector has a simple form such that the collector is very large in comparison with the entrance window, no collision to side wall occurs and therefore S_0 (θ) can be constant. The discussion which will be done in the below assumes the constant S_0.

Introducing new variables such as

$$
\left.
\begin{aligned}
u &= v_x - v_{x0} \\
t &= v_z - v_{z0} \\
\xi &= \cos\Theta = \frac{v_{z0}}{V_b}
\end{aligned}
\right\}
\tag{A8}
$$

Eq. (A5) is written as

$$
N_{\text{out}} = \tilde{A} S_0 \int_{-V_b}^{W-V_b\xi} dt \int_{-\infty}^{\infty} du \int_{-\infty}^{\infty} dv_y \exp\{-\alpha(u^2 + v_y^2 + t^2)\} \cdot (t + V_b\xi) \tag{A9}
$$

Since we know

$$
\int_{-\infty}^{\infty} e^{-\alpha u^2} du = \sqrt{\frac{\pi}{\alpha}}, \qquad \int t e^{-\alpha t^2} dt = -\frac{1}{2\alpha} e^{-\alpha t^2}
$$

We get

$$
\begin{aligned}
N_{\text{out}} = \sqrt{\frac{\alpha}{\pi}} N_0 S_0 \Bigg[V_b\xi \int_{-V_b\xi}^{W-V_b\xi} \exp(-\alpha t^2) dt \\
+ \frac{1}{2\alpha}\{\exp(-\alpha V_b^2\xi^2) - \exp(-\alpha(W - V_b\xi)^2\} \Bigg]
\end{aligned}
\tag{A10}
$$

The angle between the direction of solar wind and Z-axis of the detector, Θ changes with the satellite spinning. Consequently N_{out} also changes with the spin rotation. The dependence of N_{out} on ξ is studied in more detail in the followings.

(i) Case 1, ($T_i=0$)

When T_i goes to zero, α becomes infinity. Therefore we get,

$$\begin{aligned} N_{\text{out}} &= \lim_{\alpha\to\infty}\sqrt{\frac{\alpha}{\pi}}N_0S_0\cdot V_b\xi\int_{-V_b\xi}^{W-V_b\xi}\exp(-\alpha t^2)dt \\ &= N_0S_0V_b\cdot\xi\cdot\theta(W-V_b\xi) \end{aligned} \tag{A11}$$

here, $\theta(x)=\begin{cases}0 & (x<0)\\ 1 & (x>0)\end{cases}$. N_{out} is shown in Fig. A-2.

(ii) Case 2, ($T_i\neq 0$)

If the thermal velocity of the solar wind ($V_{th}=1/\sqrt{\alpha}$) is small compared to V_b and W, we can get $\sqrt{\alpha}V_0\gg 1$ and $\sqrt{\alpha}W\gg 1$.

(a) If $V_b\xi\gg W$, then $N_{\text{out}}\approx 0$ (A12)

(b) If $V_b\xi\ll W$, then

$$\begin{aligned} V_b\xi\int_{-V_b\xi}^{W-V_b\xi}\exp(-\alpha t^2)dt &\sim V_b\xi\int_{-\infty}^{\infty}\exp(-\alpha t^2)dt \\ &\sim V_b\xi\sqrt{\frac{\pi}{\alpha}}\gg\frac{1}{\alpha} \end{aligned}$$

Therefore we get from eq. A10

$$N_{\text{out}}\sim N_0S_0V_b\xi \tag{A13}$$

These results of (a) and (b) are the same as the case of (i).

(c) If $V_b\xi$ is comparable to W, finite temperature of the solar wind strongly influences N_{out}.

From (A10) we get

$$\frac{d}{d\xi}N_{\text{out}}=\sqrt{\frac{\alpha}{\pi}}N_0S_0\left[-WV_b\exp\{-\alpha(W-V_b\xi)^2\}+V_b\int_{-V_b\xi}^{W-V_b\xi}\exp(-\alpha t^2)dt\right] \tag{A14}$$

$$\frac{d^2}{d\xi^2}N_{\text{out}}=\sqrt{\frac{\alpha}{\pi}}N_0S_0V_b^2[\{-2\alpha W(W-V_b\xi)-1\}\exp\{-\alpha(W-V_b\xi)^2\}+\exp(-\alpha V_b^2\xi^2)] \tag{A15}$$

The solution of $(d^2/d\xi^2)N_{\text{out}}=0$ is obtained from eq. (A15) as

$$2\alpha W(W-V_b\xi)+1=\frac{\exp(-\alpha V_b^2\xi^2)}{\exp\{-\alpha(W-V_b\xi)^2\}} \tag{A16}$$

from which

$$V_b\xi = W\left\{1+0\left(\frac{1}{\alpha W^2}\right)\right\} \approx W \tag{A17}$$

Eq. (A14) beomes,

$$\left.\frac{d}{d\xi}N_{\text{out}}\right|_{V_b\xi=W} = \sqrt{\frac{\alpha}{\pi}}N_0S_0\left\{-WV_b+V_b\int_{-V_b\xi}^{0}\exp(-\alpha t^2)dt\right\}$$
$$\cong\sqrt{\frac{\alpha}{\pi}}N_0S_0V_b\left(-W+\frac{1}{2}\sqrt{\frac{\pi}{\alpha}}\right) \tag{A18}$$

Since $\sqrt{\alpha}W \gg 1$, the above equation is further changed to

$$\cong -\sqrt{\frac{\alpha}{\pi}}N_0S_0V_bW$$

If we plot N_{out} versus ξ, the maximum value of the inclination is equal to $\sqrt{\alpha/\pi}N_0S_0V_bW$. If N_0 and V_b are known, eq. (A18) gives temperature $T_i(=m_i/2k\alpha)$.

The spin axis of MS-T5 will be controlled to be perpendicular to the orbital plane. This implies that the spin axis is almost perpendicular to the solar wind flow. The central axis of the detector is, on the other hand, perpendicular to the spin axis. Consequently, Θ, the angle between the central axis and the solar wind is

$$\xi = \cos\Theta = \cos\omega t \tag{A19}$$

here, ω is angular frequency of spin rotation. Although the output data N_{out} is obtained as a function of time t, by using (A19) we can know N_{out} as a function of ξ. The results may be such as drawn in Fig. A-2.

In Fig. A-3 at the inflexion point (point A), ξ is equal to W/V_b and $(dN_{\text{out}}/d\xi)$ is equal to $-\sqrt{\alpha/\pi}\cdot N_0S_0V_bW$. Furthermore, tangent line at $\xi=0$ intersects with $\xi=W/V_b$ at the point B, where N_{out} is equal to N_0S_0W.

It is clear from above discussion that three quantities of W/V_b, N_0S_0W and $\sqrt{\alpha}N_0S_0V_bW$

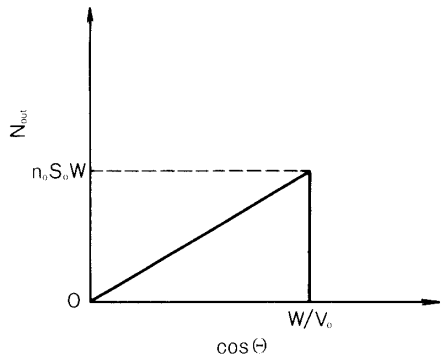

Fig. A2. Amplitude of ac ion current versus satellite rotation angle when $T_i=0$.

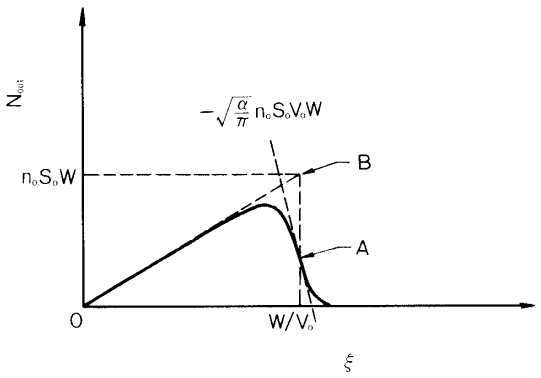

Fig. A3. Amplitude of ac current versus satellite rotation angle when $T_i \neq 0$.

are obtained from the Faraday cup on board MS-T5. Since W and S_0 are known, we can get density N_0, bulk velocity V_b and ion temperature T_i of the solar wind plasma.

References

[1] A. Bonneetti, H. S. Bridge, A. J. Lazarus, B. Rossi, and F. Scherb, Explorer 10 plasma measurement *68*, 4017–4061, J. Geophys. Res., 1963.

[2] Scherb, F., Velocity distribution of the interplanetary plasma detected by Explorer 10, 797–817, Space Res. IV, 1963.

[3] S. J. Bame, J. R. Asbridge, H. E. Helthauser, J. P. Glore, H. L. Hawk and J. Chavez, ISEE-C solar wind plasma experiment, IEEE Transactions on geoscience electronics, Vol. GE-16, *3*, 160–194, 1978.